Influence of pressure on the slow and fast fractional relaxation dynamics in lysozyme: A simulation study

Vania Calandrini[1,3,a)] and Gerald R. Kneller[1,2,3,b)]
[1]*Centre de Biophysique Moléculaire, CNRS, Rue Charles Sadron, 45071 Orléans, France*
[2]*University of Orléans, Chateau de la Source-Av. du Parc Floral, 45067 Orlans, France*
[3]*Synchrotron Soleil, L'Orme de Merisiers, B.P. 48, 91192 Gif-sur-Yvette, France*

(Received 28 September 2007; accepted 5 December 2007; published online 8 February 2008)

The article reports on a molecular dynamics simulation study of the influence of moderate, nondenaturing pressure on the slow and fast internal relaxation dynamics of lysozyme. The model parameters of the fractional Ornstein–Uhlenbeck process are used to quantify the changes. We find that the nonexponential character for diffusive motions on time scales above 10 ps is enhanced and that the diffusion processes are slowed down. The diffusive motions on the subpicosecond time scale appear, in contrast, accelerated, whereas the nonexponential character is not altered by pressure. We attribute these findings to the different natures of slow and fast relaxation processes, which are characterized by structural rearrangements and collisions, respectively. The analyses are facilitated by the use of spatially resolved relaxation rate spectra. © *2008 American Institute of Physics*. [DOI: 10.1063/1.2828769]

I. INTRODUCTION

Over the last twenty years, the use of pressure as a probe to investigate the dynamics-function relationships in biological systems has gained increasing attention in biology and biophysics.[1] From a biological point of view, the impact of pressure is, for example, of interest in studies of the adaptation of living organism to extreme conditions, as they occur at the deep sea level. One observes also that high hydrostatic pressure can be used to modulate kinetics and thermodynamics of protein aggregation.[2] In a medical context, pressure plays an important role in the formation of amyloid fibrils, which cause the Creutzfeld–Jacob syndrome, Alzheimer's, and Parkinson's disease.[3,4] We mention finally that the pressure allows us to inactivate viruses, which has motivated biotechnological applications in the field of vaccine development and virus sterilization.[5]

From a biophysical point of view, pressure plays also an important role in crystallographic and NMR studies of proteins, which permit us to explore structural changes of biomolecules on the atomic level.[6–9] Pressure-induced volume changes are of great importance in studies of protein folding and protein association[10–12] and allow us, in particular, to isolate folding intermediates that are crucial in the protein-nucleic acid recognition mechanism.[13] The application of pressure allows for a fine-tuned exploration of the energy landscape through small volume changes. In this context, we refer to a recent molecular dynamics (MD) simulation study of lysozyme, where the effect of pressure on the elasticity and on the form of local minima of the potential energy has been examined.[14]

The effect of nondenaturing pressure on the dynamics of a globular protein has been recently studied for the case of lysozyme, combining MD simulations and quasielastic neutron scattering (QENS).[15,16] Both complementary techniques have been used to access the atomic dynamics occurring on the pico- to nanosecond time scale. This work evidenced that on the observed subnanosecond time scale, pressure leads to a slowing down of protein dynamics. In the present article, we perform a more systematic, space and time-scale resolved study of pressure-induced changes in protein dynamics. Intuitively, one can imagine different scenarios after a pressure increase: (a) Reducing the volume leads to an increase of the collision frequency among nearest atoms and, thus, to an acceleration of the corresponding relaxation processes. (b) Reducing the volume causes increasingly hindered structural rearrangement of large moieties of the system, leading to a slowing down of the corresponding relaxation dynamics. We claim that, depending on the time and space scale, the former or the latter mechanism is seen.

To verify the above hypothesis, we compare by MD simulations the effect of pressure upon the internal dynamics of lysozyme on the subpicosecond and subnanosecond time scales. For both time scales, we calculate the time-dependent mean square displacement (MSD) and the single-particle intermediate scattering function correspondingly to a spatial observation scale ranging from the size of the whole protein down to a fraction of ångström. The analysis of simulation data has been performed by employing the concepts of fractional Brownian dynamics, also referred to as anomalous diffusion, which leads to an algebraic decay of the relevant correlation functions[17] and to self-similarity of the latter on the time scale. This feature has been observed before by other techniques, which allow us to monitor the functional dynamics of proteins on much longer time scales, ranging from microseconds to hours. We mention here fluorescence correlation spectroscopy and kinetic studies.[18–22] An earlier MD study has revealed that fractional Brownian dynamics is

a)Electronic mail: gerald.kneller@cnrs-orleans.fr.
b)Electronic mail: vania.calandrini@cnrs-orleans.fr.

already developed on the much shorter nanosecond time scale, which is accessible to MD simulations and to neutron scattering techniques.[23] The fractional Ornstein–Uhlenbeck (OU) process is a particularly simple model which describes the anomalous diffusion of a Brownian particle in a harmonic potential. It has been shown in Ref. 24 that the model yields a satisfactory description of incoherent QENS spectra and corresponding computer simulation results. The same model has been used in our previous works on the influence of hydrostatic pressure on the internal dynamics of lyzozyme, by MD simulations and QENS experiments.[15,16] In the framework of this model, we give here an analytical expression for the spatially resolved relaxation rate spectra which are useful to describe the characteristics of the relaxation dynamics of protein.

The paper is organized as follows. Sections II and III contain, respectively, a short description of the MD simulations and a presentation of the analytical model which is used to interpret the simulation data. In Sec. IV, we present the analyses of MD simulations and the results. Section V concludes the paper by a short résumé.

II. SIMULATIONS

Molecular dynamics simulations have been performed for a system consisting of one lysozyme molecule surrounded by 3403 water molecules, using the program package MMTK (Ref. 25) with the AMBER94 force field.[26] The system was enclosed in a rectangular box of an average size of $6.15\times4.10\times4.61$ nm^3, applying periodic boundary conditions. The lysozyme structure was taken from the Brookhaven protein databank[27] [code 193L (Ref. 28)], and hydrogen atoms were added to the structure according to standard criteria concerning the chemical bond structure of amino acids. To mimic realistic thermodynamic conditions, the system was simulated in the thermodynamics NpT ensemble, employing the extended system method[29,30] with an integration time step of 0.001 ps. The effective masses of the thermostat and the barostat were chosen such that the corresponding characteristic time constants were 0.2 and 1.5 ps, respectively.

In order to account for long-range electrostatic interactions in an efficient way, a modified Ewald summation procedure has been used to compute electrostatic forces and energies.[31] To analyze the dynamics on the subnanosecond and subpicosecond time scales, we created, respectively, a trajectory of 20 ps with a sampling step of 0.005 ps and a trajectory of 1 ns with a sampling step of 0.04 ps. In the following, we refer to the two dynamical regimes as "fast" and "slow," respectively. To be able to study the internal protein dynamics, global translations and rotations of the lysozyme molecule have been subtracted by superposing its configuration for each time frame with the corresponding initial configuration.[32]

III. MODELING THE SINGLE-PARTICLE DYNAMICS

To interpret the MD simulations, we used the fractional Ornstein–Uhlenbeck process as model for the dynamics of one tagged, "representative" atom. Knowing that incoherent scattering from hydrogen is the predominant scattering type from biological samples, the tagged atom can be identified with a hydrogen atom.

A. Time-dependent mean square displacement

The basic quantity to study in the analysis of diffusive internal protein dynamics is the time-dependent MSD,

$$W(t) := \langle [\mathbf{R}(t) - \mathbf{R}(0)]^2 \rangle. \tag{1}$$

Here, $\mathbf{R}$ contains the Cartesian components of the position vector of a tagged, diffusing atom and the brackets indicate a thermal average. Assuming thermal equilibrium, spatially confined motions, and isotropy, one may write $W(t)=6(\langle x^2\rangle - \langle x(t)x(0)\rangle)$, where x is one Cartesian coordinate of the position of the tagged atom. Since the position autocorrelation function $\langle x(t)x(0)\rangle$ tends to zero for $t\to\infty$, the MSD tends to a finite plateau value, $\lim_{t\to\infty} W(t)=6\langle x^2\rangle$. The plateau value is, thus, determined by the mean position fluctuation, $\langle x^2\rangle$.

In the framework of the fractional OU process, one has[17]

$$\langle x(t)x(0)\rangle = \langle x^2\rangle E_\alpha(-[t/\tau]^\alpha), \quad 0<\alpha\leqslant 1, \tag{2}$$

and definition (1) yields

$$W(t) = 6\langle x^2\rangle(1 - E_\alpha(-[t/\tau]^\alpha)). \tag{3}$$

Here, $E_\alpha(z)$ is the Mittag–Leffler function[33]

$$E_\alpha(z) = \sum_{k=0}^{\infty} \frac{z^k}{\Gamma(1+\alpha k)}, \tag{4}$$

where $\Gamma(\cdot)$ denotes the generalized factorial.[34] The Mittag–Leffler function is an entire function, which is analytic everywhere in the complex plane and represents a generalization of the exponential function. One sees easily that $E_1(z)=\Sigma_{k=0}^{\infty} z^k/k!=\exp(z)$. For $\alpha=1$, expression (2) yields, thus, the exponentially decaying position autocorrelation function of the normal OU process,[35–37] whereas $\alpha<1$ leads to "anomalous," non-Markovian diffusion with long-time memory effects.[23]

B. The intermediate scattering function

We consider now the single-particle intermediate scattering function, whose Fourier spectrum is measured by quasielastic neutron scattering experiments,

$$I(q,t) = \langle \exp(iq[x - x_0]) \rangle. \tag{5}$$

Here, $q=|\mathbf{q}|$ is the modulus of the momentum transfer which the neutron transfers to scattering atom. Within the model of the fractional OU process, the intermediate scattering function takes the form[24]

$$I(q,t) = \exp(-q^2\langle x^2\rangle) \sum_{n=0}^{\infty} \frac{q^{2n}\langle x^2\rangle^n}{n!} E_\alpha(-[t/\tau_n]^\alpha), \quad 0<\alpha\leqslant 1, \tag{6}$$

where τ_n is given by

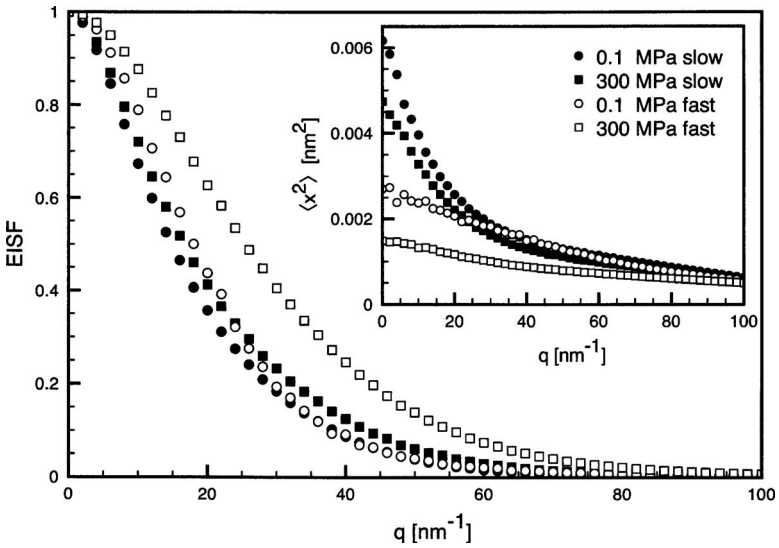

FIG. 1. Simulated EISF of lysozyme for $p=0.1$ and 300 MPa obtained from the short trajectory (20 ps, $\Delta t = 0.005$ ps→fast) and from the long trajectory (1 ns, $\Delta t = 0.040$ ps→slow) (Ref. 16). The inset shows the position fluctuations derived from expression (10).

$$\tau_n = \tau n^{-1/\alpha}. \tag{7}$$

For $\alpha=1$, the intermediate scattering function of the normal Ornstein–Uhlenbeck process is retrieved, which may be cast into the form[24]

$$I_{\mathrm{OU}}(q,t) = \lim_{\alpha\to 1} I(q,t) = \exp(-q^2\langle x^2\rangle[1-\exp(-t/\tau)]). \tag{8}$$

To obtain Eq. (8) from Eq. (6), it has been used that $\exp(-nt/\tau)=(\exp[-t/\tau])^n$. We note that a corresponding relation does not exist for Mittag–Leffler functions, which means that expression (6) cannot be further simplified.

In the limit of $t\to\infty$, relation (6) yields the elastic incoherent structure factor (EISF),

$$\mathrm{EISF}(q) := \lim_{t\to\infty} I(q,t) = \exp(-q^2\langle x^2\rangle), \tag{9}$$

which has Gaussian form. In general, the Gaussian approximation holds strictly only for $q\to 0$,[38] and MD simulations allow us to verify the hypothesis of a Gaussian model for the EISF. In Fig. 1, the simulated EISF is shown for the two pressures considered in this article and for both time regimes. Assuming that the Gaussian approximation holds, the definition

$$\langle x^2\rangle = -\ln(\mathrm{EISF}[q])/q^2 \tag{10}$$

should lead to a constant atomic mean square position fluctuation. The inset of Fig. 1 shows clearly that this is not the case. This does, however, not necessarily mean that the Gaussian approximation does not hold, but only that the Gaussian approximation is not compatible with the assumption of one single representative scattering atom. It has, in fact, been shown that the Gaussian model of coupled harmonic oscillators with friction can represent the EISF of a protein up to moderate q values, since such a model can account for motional heterogeneity.[39] In the following, the parameters of the fractional OU process are, thus, considered q-dependent. Another feature to be observed is that, as expected, both the EISF and the atomic mean square position fluctuation obtained from MD simulations depend on the observation time scale.

C. Relaxation rate spectrum for $I(q,t)$

In order to quantify the nonexponential character of the intermediate scattering function (6), we represent the latter in terms of a superposition of normal exponential functions,

$$I(q,t) = \int_0^\infty d\lambda p_{\alpha,\tau,q}(\lambda)\exp(-\lambda t), \tag{11}$$

where $p_{\alpha,\tau,q}(\lambda)\geqslant 0$. Since $I(q,0)=1$, $p_{\alpha,\tau,q}(\lambda)$ is normalized to 1,

$$\int_0^\infty d\lambda p_{\alpha,\tau,q}(\lambda) = 1. \tag{12}$$

The relaxation rate spectrum $p_{\alpha,\tau,q}(\lambda)$ can be obtained by an inverse Stieltjes transform[40] of the Laplace transformed intermediate scattering function $\hat{I}(q,s)$,

$$p_{\alpha,\tau,q}(\lambda) = \lim_{\epsilon\to 0^+} \frac{1}{\pi}\Im\{\hat{I}(q,-[\lambda+i\epsilon])\}. \tag{13}$$

In the case of the fractional OU process, $\hat{I}(q,s)$ takes the form

$$\hat{I}(q,s) = \exp(-q^2\langle x^2\rangle)\left(\frac{1}{s}+\sum_{n=1}^{\infty}\frac{q^{2n}\langle x^2\rangle^n}{n!}\frac{1}{s(1+n(s\tau)^{-\alpha})}\right) \tag{14}$$

and the distribution function reads as

$$p_{\alpha,\tau,q}(\lambda) = \exp(-q^2\langle x^2\rangle)\left(\delta(\lambda)+\sum_{n=1}^{\infty}\frac{q^{2n}\langle x^2\rangle^n}{n!}g_{\alpha,\tau,n}(\lambda)\right), \quad 0<\alpha<1, \tag{15}$$

where

$$g_{\alpha,\tau,n}(\lambda) = \frac{\tau}{\pi}\frac{(\tau\lambda)^{\alpha-1}\sin(\pi\alpha)}{(\tau\lambda)^{2\alpha}n^{-1}+2(\tau\lambda)^{\alpha}\cos(\pi\alpha)+n}, \quad n=1,2,\ldots, \tag{16}$$

is the relaxation rate spectrum relevant to the Mittag–Leffler function $E_\alpha(-n[t/\tau]^\alpha)$. One finds from Eq. (14) that the dis-

tribution function takes the form of a superposition of discrete peaks in case that $\alpha=1$,

$$p_{1,\tau,q}(\lambda) = \exp(-q^2\langle x^2\rangle)\sum_{n=0}^{\infty}\frac{q^{2n}\langle x^2\rangle^n}{n!}\delta(\lambda - n/\tau). \quad (17)$$

IV. DATA ANALYSIS AND RESULTS

A. Fitting simulated time correlation functions

To compute MSDs and time correlation functions from MD trajectories, we used the MD analysis package NMOLDYN.[41] The calculations have been carried out by averaging over individual atomic contributions, weighting each atom according to its incoherent neutron scattering cross section. Due to the predominant incoherent scattering of hydrogen, this amounts in practice to perform equally weighted averages over the hydrogen atoms. In order to fit expressions (3) and (6) to their corresponding simulated counterparts, one needs to evaluate functions of the type $E_\alpha(-n[t/\tau]^\alpha)$. Since the series [Eq. (4)] converges slowly for large arguments, we used their integral representation based on the relaxation rate spectrum. This procedure has proven to be satisfactory in Ref. 16. Starting from the decomposition [Eq. (16)] and performing the variable change $nu=(\lambda\tau)^\alpha$, one obtains

$$E_\alpha(-n[t/\tau]^\alpha) = \frac{1}{\pi\alpha}\int_0^\infty du\frac{\sin(\pi\alpha)}{u^2+2u\cos(\pi\alpha)+1} \times\exp(-(nu)^{1/\alpha}t/\tau), \quad (18)$$

where the integral is evaluated numerically.

B. Results and discussion

1. Mean square displacement

Figure 2 displays the time evolution of the simulated MSD and the fit of expression (3) for both dynamical regimes at both pressures ($p=0.1$ MPa and 300 MPa). Here, $\langle x^2\rangle$ is not a fit parameter but a fixed value which is obtained from the corresponding EISF data via relation (10) in the limit of $q\to 0$. The fit parameters α and τ are summarized in Tables I and II. Our data show that

(1) as expected, the configurational space explored by atomic motions seen for the fast dynamical regime is reduced with respect to the one explored over longer time scales and pressure reduces in both cases the motional amplitudes;
(2) pressure leads to a slowing down of the relaxation dynamics seen for the slow dynamical regime, while it leads to an acceleration for the fast one; and
(3) the fractional characteristics of the MSD for both dynamical regimes are similar ($\alpha\approx 0.5$ for the slow regime and $\alpha\approx 0.6$ for the fast one) and are not affected by pressure. We note here that $\alpha<1$ indicates a "subdiffusive" evolution of the MSD for short times, where the latter grows slower than linearly. From a mathematical point of view, this effect can be explained by a position autocorrelation function, which is described by a superposition of exponential functions with a large spectrum of relaxation rates. The origin of this heterogeneity can be static or dynamic. As for the static heterogeneity, we recall that the simulated MSDs represent an average over all atoms in the protein. Even if the atomic autocorrelation functions decay exponentially, one obtains a nonexponentially decaying average correlation function if the individual relaxation rates are not all the same. The dynamical heterogeneity, on the contrary, arises from a superposition of different relaxation channels for a given atomic autocorrelation function. In a protein, both static and dynamical heterogeneities of the atomic motions have to be considered, since each atom moves in a different environment and all degrees of freedom are strongly coupled.

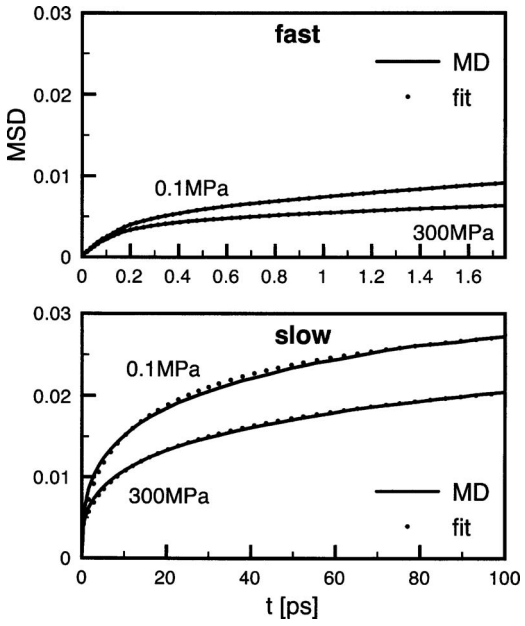

FIG. 2. Average atomic mean square displacement of lysozyme in solution obtained from MD simulation at $p=0.1$ and at 300 MPa (solid lines). The broken lines correspond to a fit of the model according to expression (3). The panel named "fast" refers to the short trajectory (20 ps, $\Delta t=0.005$ ps) and the one named "slow" to the long trajectory (1 ns, $\Delta t=0.040$ ps) (Ref. 16) (see Tables I and II for the resulting parameters).

We note here that the simulated MSDs do not tend correctly to a plateau value for large times (not shown here), since very low frequency motions are not sufficiently well sampled due to the finite lengths of the underlying MD trajectories. Therefore, the model fits have been performed using only the statistically safe part of the simulated MSDs ($t<0.1T$, with T being the length of the corresponding MD trajectory). The MSD analysis suggests that, depending on the observed time scale, different relaxation mechanisms contribute to the internal dynamics of proteins, which are differently affected by pressure.

2. Intermediate scattering function

To gain more insight into the mechanisms underlying the relaxation dynamics seen for both dynamical regimes, we carried out an analysis of the intermediate scattering function and of the corresponding relaxation rate spectrum, which al-

TABLE I. Parameters for the fractional Ornstein–Uhlenbeck process obtained from fits to the simulated MSDs and to the simulated intermediate scattering functions obtained from the short trajectory (20 fs, $\Delta t=0.005$ ps). The value of $\langle x^2\rangle$ is fixed according to Eq. (10).

	0.1 MPa			300 MPa		
	$\langle x^2\rangle$ (nm^2)	α	τ (ps)	$\langle x^2\rangle$ (nm^2)	α	τ (ps)
MSD	2.70×10^{-3}	0.59	2.02	1.49×10^{-3}	0.60	0.81
$I_{\mathrm{inc}}(6/\mathrm{nm}^{-1},t)$	2.57×10^{-3}	0.61	1.63	1.43×10^{-3}	0.60	0.75
$I_{\mathrm{inc}}(10/\mathrm{nm}^{-1},t)$	2.37×10^{-3}	0.63	1.39	1.32×10^{-3}	0.64	0.58
$I_{\mathrm{inc}}(20/\mathrm{nm}^{-1},t)$	2.07×10^{-3}	0.65	1.05	1.17×10^{-3}	0.66	0.45
$I_{\mathrm{inc}}(40/\mathrm{nm}^{-1},t)$	1.49×10^{-3}	0.75	0.51	8.76×10^{-4}	0.77	0.26
$I_{\mathrm{inc}}(50/\mathrm{nm}^{-1},t)$	1.28×10^{-3}	0.80	0.39	7.88×10^{-4}	0.80	0.22
$I_{\mathrm{inc}}(80/\mathrm{nm}^{-1},t)$	7.68×10^{-4}	0.90	0.18	6.03×10^{-4}	0.88	0.16

lows for a characterization of relaxation processes in reciprocal space. The intermediate scattering function has been calculated for both time scales at different q values between $q=6$ and 80 nm^{-1}, corresponding, respectively, to a spatial observation scale of the size of the whole lysozyme molecule and to $\approx$0.1 nm. The model [Eq. (6)] is fitted to the data by using up to 12 terms of the series. As already indicated, the position fluctuation is obtained from the EISF via expression (10) (data shown in the inset of Fig. 1). The fitted values for α and τ are listed in Tables I and II. Figures 3 and 4 show the intermediate scattering functions calculated for fast and slow dynamical regimes, respectively. The intermediate scattering functions are displayed together with the fitted model functions for $q=6$ and 50 nm^{-1} and two pressures. We remark that the analytical model based on the fractional OU process yields good fits even on the subpicosecond time scale.

The q-dependent parameters τ and α are resumed in Fig. 5. The values for $q=0$ correspond to the mean square displacements. As for the slow dynamical regime, the evolution of τ shows that the pressure generally leads to a slowing down of the relaxation dynamics, which is most pronounced at low q values. This indicates that large scale motions are particularly concerned. The effect disappears for $q \geqslant 40$ nm^{-1}, corresponding to motions localized within a radius of about 1.5 Å. In the case of the fast dynamical regime, pressure leads, on the contrary, again to an acceleration of the relaxation dynamics. The effect progressively decreases with increasing q, i.e., with increasing localization of the observed motions. These findings suggest the presence of two relaxation mechanisms which are differently affected by the application of pressure:

(a) fast and localized diffusive motions, which are accelerated. We consider this type of motion to be collision dominated and, thus, accelerated since the mean free path is reduced.
(b) slower diffusive motions on larger space scales which are slowed down since they require large scale spatial rearrangements which are increasingly hindered under pressure.

It is important to note that slow dynamical regime contains also motions of type (a), which are, however, not resolved with the same sampling time step used in the fast dynamical regime. Increasing the value of q in the intermediate scattering function, one focuses the view on fast localized motions, excluding motions of type (b). We think that this is the reason why the parameter τ at high q values is essentially the same for both dynamical regimes. We attribute the observation that the influence of pressure disappears, too, for high q values to the fact that extremely localized motions reflect the atomic momentum distribution which is not influenced by pressure.

The difference in the relaxation mechanisms seen for the two dynamical regimes is also reflected in the nonexponential behavior of the corresponding intermediate scattering

TABLE II. Parameters for the fractional Ornstein–Uhlenbeck process obtained from fits to the simulated MSDs and to the simulated intermediate scattering functions obtained from the long trajectory (1 ns, $\Delta t=0.040$ ps). The value of $\langle x^2\rangle$ is fixed according to Eq. (10).

	0.1 MPa			300 MPa		
	$\langle x^2\rangle$ (nm^2)	α	τ (ps)	$\langle x^2\rangle$ (nm^2)	α	τ (ps)
MSD	6.17×10^{-3}	0.54	31.75	4.74×10^{-3}	0.54	39.08
$I_{\mathrm{inc}}(6/\mathrm{nm}^{-1},t)$	4.68×10^{-3}	0.53	13.48	3.94×10^{-3}	0.50	19.43
$I_{\mathrm{inc}}(10/\mathrm{nm}^{-1},t)$	3.96×10^{-3}	0.51	8.86	3.28×10^{-3}	0.49	13.58
$I_{\mathrm{inc}}(20/\mathrm{nm}^{-1},t)$	2.57×10^{-3}	0.52	2.53	2.21×10^{-3}	0.45	4.39
$I_{\mathrm{inc}}(22/\mathrm{nm}^{-1},t)$	2.41×10^{-3}	0.50	2.3	2.08×10^{-3}	0.44	3.64
$I_{\mathrm{inc}}(40/\mathrm{nm}^{-1},t)$	1.52×10^{-3}	0.59	0.63	1.30×10^{-3}	0.47	0.72
$I_{\mathrm{inc}}(50/\mathrm{nm}^{-1},t)$	1.30×10^{-3}	0.66	0.45	1.12×10^{-3}	0.51	0.46
$I_{\mathrm{inc}}(80/\mathrm{nm}^{-1},t)$	8.68×10^{-4}	0.92	0.26	7.72×10^{-4}	0.84	0.24

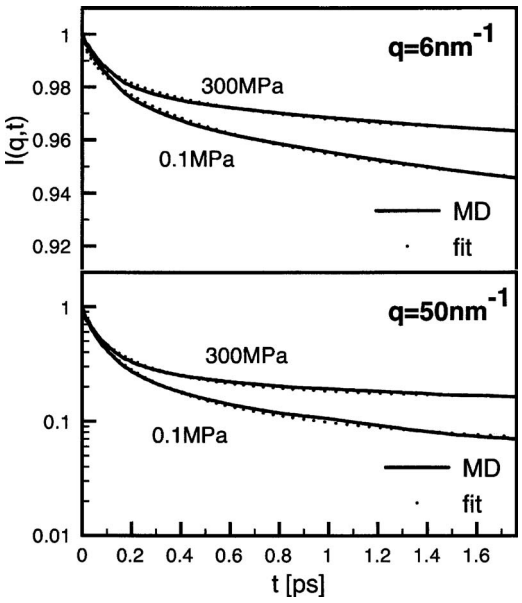

FIG. 3. Simulated incoherent intermediate scattering function (solid lines) obtained from the short trajectory (20 ps, Δt=0.005 ps) and fit of expression (6) (broken lines) for p=0.1 and 300 MPa at q=6 nm^{-1} (upper part) and 50 nm^{-1} (lower part). The parameters are given in Table I.

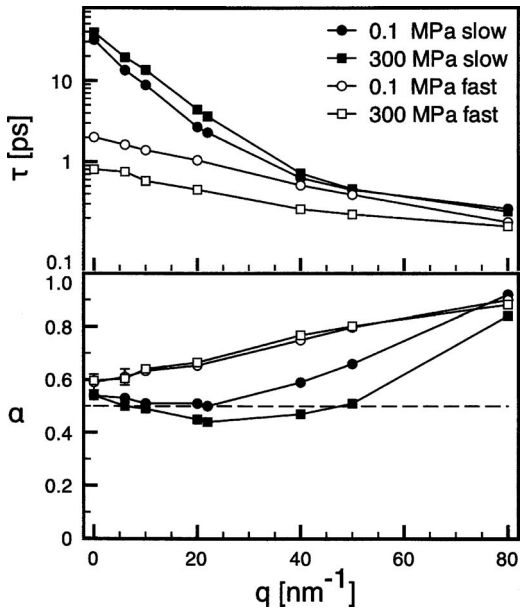

FIG. 5. Fitted model parameters τ and α for both time scales (slow$\rightarrow t$ =1 ns, Δt=0.040 ps and fast$\rightarrow t$=20 ps, Δt=0.005 ps) as a function of q for p=0.1 and 300 MPa.

functions, which is described by the parameter α (bottom of Fig. 5). One observes that the parameter α is, in general, lower for the slow dynamical regime. We think that this is a consequence of the lengths of the analyzed trajectories. The longer one exhibits more dynamical heterogeneity than the shorter one, simply because a tagged particle has more time to explore different conformational substates, following motions of type (b) which are superposed to the faster diffusive motions of type (a). The hypothesis that the longer trajectory describes a superposition of two relaxation processes (a) and (b), while the shorter one resolves only type (a), is supported by the observation that the difference in the fractional behavior between the corresponding intermediate scattering functions disappears progressively with increasing localization of the observed motions, i.e., with increasing q values, where the slow large amplitude relaxation mechanisms are not seen. At the same time, one observes with increasing q that the parameter α tends to 1, i.e., a tendency toward exponential

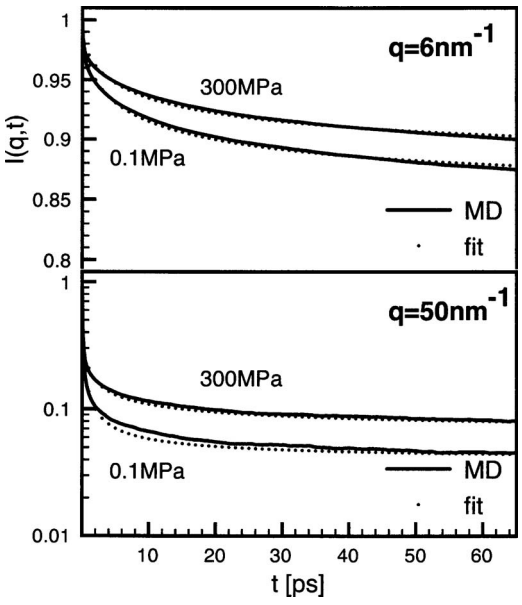

FIG. 4. Simulated incoherent intermediate scattering function (solid lines) obtained from the long trajectory (1 ns, Δt=0.040 ps) and fit of expression (6) (broken lines) for p=0.1 and 300 MPa at q=6 nm^{-1} (upper part) and 50 nm^{-1} (lower part). The parameters are given in Table II.

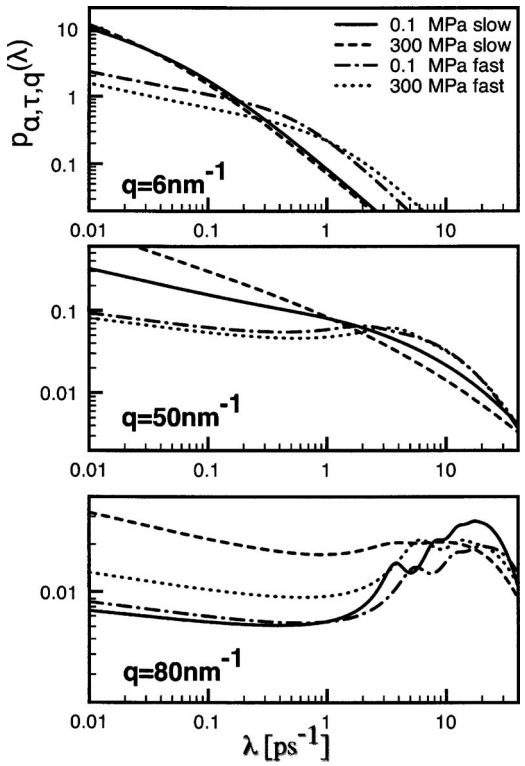

FIG. 6. Distribution functions associated with the intermediate scattering functions calculated according to expression (15) using the parameters in Tables I and II.

relaxation. This indicates again a "loss" of relaxation channels corresponding to large amplitude motions. We recall that the static heterogeneity of the motions, which is due to the fact that each atom is in an specific environment, must be considered as a sort of background effect in this context.

Concerning the influence of pressure on the fractional characteristics of the relaxation dynamics, one observes first of all that the parameter α does not change for the fast dynamical regime, while strongly q-dependent differences can be seen for the slow dynamical regime. Looking at the general evolution of α with q for the slow dynamical regime, one observes that the pressure has no influence for $q=0$. For higher q values, however, pressure leads effectively to a shift of $\alpha(q)$ toward higher q values, which can be attributed to an enhanced localization of the particle motions. The effect can be quantified through the q-dependent relaxation rate spectra shown in Fig. 6. One sees clearly increasing pressure leads, for a given q value, to an increase of the weights of slow relaxation rates and a corresponding lowering of α. For the fast regime, this effect is not observed because the observation time is not sufficient to explore the additional slower decay channels.

V. CONCLUSIONS

We have presented a comprehensive MD simulation study of the effect of nondenaturing hydrostatic pressure on the diffusive single-atom dynamics in lysozyme. The impact of pressure was studied on two different time scales, using the fractional Ornbstein–Uhlenbeck process as a dynamical model to interpret the results at different spatial scales. We showed that the validity of the model can be extended to the subpicosecond time scale, as far as single-particle diffusion is concerned. To facilitate the analysis, we introduced the relaxation rate spectrum of the intermediate scattering function, which allows for a spatially resolved characterization of relaxation processes.

Apart from a reduction of the atomic position fluctuations under pressure, which was observed for both fast and slow dynamical regimes, the simulations show that the relaxation dynamics is driven by two different mechanisms: (a) fast and localized diffusive motions, which are collision dominated, and (b) slower diffusive motions on larger space scales which involve large conformational rearrangements. The above mechanisms are differently affected by pressure; motions of type (a) are accelerated since the mean free path is reduced, leading thus to an increasingly number of collisions among nearest neighboring atoms, while motions of type (b) are slowed down since large scale rearrangements are increasingly hindered under pressure, due to the increase of atomic packing density. Schematically, one can say that the dynamics relevant to the fast dynamical regime essentially is dominated by motions of type (a), while the relaxation dynamics seen in the slow dynamical regime results from a superposition of motions of types (a) *and* (b). The dynamical heterogeneity, due to the superposition of many motions, and the structural heterogeneity in the protein, i.e., environmental effects concerning individual atoms, are responsible for the nonexponential behavior of the relaxation dynamics.

As for the impact of pressure on the nonexponential behavior of slow and fast dynamical regimes, our data suggest that the pressure affects essentially slower motions which imply structural rearrangements. Our analyses of the incoherent intermediate scattering function, which give access to a spatial Fourier decomposition of single-particle motions, reveal that the reduction of the motional amplitudes is reflected in an increased nonexponential relaxation. For a fixed spatial scale, this effect is, however, only visible if one follows the dynamics of the particle for long enough times.

ACKNOWLEDGMENTS

V. Calandrini acknowledges financial support by the Agence Nationale de la Recherche (Contract no. ANR-06-CIS6-012-01) and the Fondazione Angelo Della Riccia.

[1] C. Balny, P. Masson, and K. Heremans, Biochim. Biophys. Acta **1595**, 3 (2002).
[2] T. Randolph, M. Seefeldt, and J. Carpenter, Biochim. Biophys. Acta **1595**, 224 (2002).
[3] F. Meersman, C. Dobson, and K. Heremans, Chem. Soc. Rev. **35**, 908 (2006).
[4] A. Roher and Y.-M. Kuo, Methods Enzymol. **309**, 58 (1999).
[5] A. Oliveira, D. Ishimaru, R. Goncalves, T. J. Smith, P. Mason, D. Sa–Carvalho, and J. Silva, Biophys. J. **76**, 1270 (1999).
[6] C. Kundrot and F. Richards, J. Mol. Biol. **193**, 157 (1987).
[7] M. Refaee, T. Tezuka, K. Akasaka, and M. Williamson, J. Mol. Biol. **327**, 857 (2003).
[8] J. Jonas, Biochim. Biophys. Acta **1595**, 145 (2002).
[9] R. Fourme, E. Girard, R. Kahn, A. Dhaussy, M. Mezouar, N. Colloc'h, and I. Ascone, Biochim. Biophys. Acta **1764**, 384 (2006).
[10] K. Frye and C. A. Royer, Protein Sci. **7**, 2217 (1998).
[11] B. B. Boonyaratanakornkit, C. Park, and D. Clark, Biochim. Biophys. Acta **1595**, 235 (2002).
[12] G. Hummer, S. Garde, A. Garcia, M. Paulatis, and L. Pratt, Proc. Natl. Acad. Sci. U.S.A. **95**, 1552 (1998).
[13] J. L. Silva, A. C. Oliveira, A. M. O. Gomes, L. M. T. R. Lima, R. Mohana–Borges, A. B. F. Pacheco, and D. Foguel, Biochim. Biophys. Acta **1595**, 250 (2002).
[14] L. Meinhold, J. Smith, A. Kitao, and A. Zewail, Proc. Natl. Acad. Sci. U.S.A. **104**, 17261 (2007).
[15] V. Hamon, P. Calligari, K. Hinsen, and G. Kneller, J. Non-Cryst. Solids **352**, 4417 (2006).
[16] V. Calandrini, V. Hamon, K. Hinsen, P. Calligari, M.-C. Bellissent–Funel, and G. Kneller, Chem. Phys. (in press).
[17] R. Metzler and J. Klafter, Phys. Rep. **339**, 1 (2000).
[18] W. Glöckle and T. Nonnenmacher, Biophys. J. **68**, 46 (1995).
[19] H. Lu, L. Xun, and X. Xie, Science **282**, 1877 (1998).
[20] H. Yang and X. Xie, J. Chem. Phys. **117**, 10965 (2002).
[21] H. Yang, G. Luo, P. Karnchanaphanurach, T. Louie, I. Rech, S. Cova, L. Xun, and X. Xie, Science **302**, 262 (2003).
[22] S. Kou and X. Xie, Phys. Rev. Lett. **93**, 180603 (2004).
[23] G. Kneller and K. Hinsen, J. Chem. Phys. **121**, 10278 (2004).
[24] G. Kneller, Phys. Chem. Chem. Phys. **7**, 2641 (2005).
[25] K. Hinsen, J. Comput. Chem. **21**, 79 (2000); See: http://dirac.enrs-orleans.fr
[26] W. Cornell, P. Cieplak, C. Bayly, I. I. R. Gould, K. Merz, Jr., D. Ferguson, D. Spellmeyer, T. Fox, J. Caldwell, and P. Kollman, J. Am. Chem. Soc. **117**, 5179 (1995).
[27] H. Berman, J. Westbrook, Z. Feng, G. Gilliland, T. Bhat, H. Weissig, I. Shindyalov, and P. Bourne, Nucleic Acids Res. **28**, 235 (2000).
[28] M. Vaney, S. Maignan, M. RiesKautt, and A. Ducruix, Acta Crystallogr., Sect. D: Biol. Crystallogr. **52**, 505 (1996).
[29] H. Andersen, J. Chem. Phys. **72**, 2384 (1980).
[30] S. Nosé, J. Chem. Phys. **81**, 511 (1984).
[31] D. Wolf, P. Keblinski, S. Philpot, and J. Eggebrecht, J. Chem. Phys. **110**, 8254 (1999).

[32] G. Kneller, Mol. Simul. **7**, 113 (1991).
[33] A. Erdélyi, W. Magnus, F. Oberhettinger, and F. Tricomi, *Higher Transcendental Functions* (McGraw-Hill, New York, 1955).
[34] M. Abramowitz and I. Stegun, *Handbook of Mathematical Functions* (Dover, New York, 1972).
[35] M. Wang and G. Uhlenbeck, Phys. Rev. **93**, 249 (1945).
[36] C. Gardiner, *Handbook of Stochastic Methods*, 2nd ed., Springer Series in Synergetics (Springer, Berlin, 1985).
[37] H. Risken, *The Fokker-Planck Equation*, 2nd ed., Springer Series in Synergetics (Springer, Berlin, 1996).
[38] J. Boon and S. Yip, *Molecular Hydrodynamics* (McGraw-Hill, New York, 1980), see Eqs. (3.5.23), (3.5.33), and (3.5.37) and the corresponding references.
[39] K. Hinsen, A.-J. Petrescu, S. Dellerue, M. Bellissent–Funel, and G. Kneller, in *Condensed Phase Structure and Dynamics: A combined neutron scattering and molecular modelling approach*, special issue of Chem. Phys. **261**, 25 (2000).
[40] J. Schwarz, J. Math. Phys. **46**, 013501 (2005).
[41] T. Rog, K. Murzyn, K. Hinsen, and G. Kneller, J. Comput. Chem. **24**, 657 (2003).